Photoacoustics 29 (2023) 100438

Contents lists available at ScienceDirect

Photoacoustics

journal homepage: www.elsevier.com/locate/pacs

Characterization of H_2S QEPAS detection in methane-based gas leaks dispersed into environment

Mariagrazia Olivieri [a], Giansergio Menduni [a], Marilena Giglio [a], Angelo Sampaolo [a,*], Pietro Patimisco [a], Hongpeng Wu [b], Lei Dong [b], Vincenzo Spagnolo [a,b]

[a] PolySense Lab - Dipartimento Interateneo di Fisica, Politecnico and University of Bari, Via Amendola 173, Bari, Italy
[b] State Key Laboratory of Quantum Optics and Quantum Optics Devices, Institute of Laser Spectroscopy, Shanxi University, Taiyuan 030006, China

ARTICLE INFO

Keywords:
Quartz-enhanced photoacoustic spectroscopy
Hydrogen sulfide
Methane
Hazardous gas leaks detection
Gas and oil wells
Environmental monitoring

ABSTRACT

The increase in fatal accidents and chronic illnesses caused by hydrogen sulfide (H_2S) exposure occurring in various workplaces is pushing the development of sensing systems for continuous and in-field monitoring of this hazardous gas. We report here on the design and realization of a Near-IR quartz-enhanced photoacoustic sensor (QEPAS) for H_2S leaks detection. H_2S QEPAS signal was measured in matrixes containing up to 1 % of methane (CH_4) and nitrogen (N_2) which were chosen as the laboratory model environment for leakages from oil and gas wells or various industrial processes where H_2S and CH_4 can leak simultaneously. An investigation of the influence of CH_4 on H_2S relaxation and photoacoustic generation was proposed in this work and the sensor performances were carefully assessed with respect to CH_4 content in the mixture. We demonstrated the high selectivity, with no cross talk between H_2S, H_2O and CH_4 absorption lines, high sensitivity, and fast response time of the developed sensor, achieving a minimum detection limit (MDL) of 2.5 ppm for H_2S with 2 s lock-in integration time. The employed 2.6 μm laser allowed us to employ the sensor also for CH_4 detection, achieving an MDL of 85 ppm. The realized QEPAS sensor lends itself to the development of a portable and compact device for industrial monitoring.

1. Introduction

Trace gas detection is among the main issues in industrial and urban area environmental monitoring, atmospheric science, and medical applications. Hydrogen sulfide (H_2S) is one of the most challenging gases to detect since it is hazardous, corrosive, and flammable even at very low concentrations. The Occupational Safety and Health Administration (OSHA, US Department of Labor) fixed at 20 part per million (ppm) the concentration limit for H_2S breathing, for an eight-hour period, with a maximum peak exposure of 50 ppm for ten minutes [1]. The National Institute for Occupational Safety and Health determined an IMDH (Immediately Dangerous to Life and Health) concentration limit of 100 ppm for H_2S. The typical rotten eggs smell, perceptible starting from concentrations of few ppm, disappears at 100 ppm and olfactory paralysis and eye irritation could occur. Exposures to concentrations higher than 500 ppm are fatal [2].

Human activity represents the main source of H_2S global emission. This gas is largely produced in coke ovens, sewerage, tanneries, pulp and paper industries [3]. H_2S concentrations ranging from few ppms to percents are found in crude oil and natural gas (NG) reservoirs [4]. A recent study on releases of methane (CH_4) and H_2S from active, abandoned and marginally producing oil and gas wells in Ontario (Canada), classifies these emissions as major risks for human and ecosystem health [5]. In addition, leakages from NG transmission pipelines systems typically occur. In their last survey, the European Gas Pipeline Incidents Data Group (EGIP) reported that the major contributions for gas pipelines leakages arise from external interferences, corrosion, construction defects or material failure, and natural disasters such as earthquakes [6]. H_2S is also found as a by-product in NG processing plants during raw NG purification and in petroleum refiners, where H_2S is produced during hydrodesulfurization of petroleum feedstocks and fuels [7].

According to the OSHA, approximately 100 accidents involving H_2S exposure (70 % of which were fatal) occurred over the last two decades in a variety of workplaces in USA, including oil and gas wells, gas and petroleum plants, sewer lines, and tanks [1]. In addition, the release of H_2S impose serious threats also for the environments and residents surrounding the leak sources [8,9]. Thereby, the development of sensors capable of real-time and continuous monitoring of H_2S leaks dispersed

* Correspondence to: Dipartimento Interateneo di Fisica, University and Politecnico of Bari, Via Amendola 173, Bari, Italy.

https://doi.org/10.1016/j.pacs.2022.100438
Received 8 October 2022; Received in revised form 20 November 2022; Accepted 8 December 2022
Available online 13 December 2022

into environment has become an urgent need. Beyond the fast response and sensitivity, the high selectivity represents the main characteristic to fulfil, provided the high probability to identify an H_2S leak source that is strictly related to a hydrocarbon-based matrix, mainly composed of CH_4.

Many techniques have been used for H_2S detection. Gas chromatography was largely exploited, but despite the high sensitivity and precision, the need for a sample preparation consisting in multiple steps makes this technique not suitable for real-time measurement and detection of short-term concentration variations [10]. Chemical sensors, such as those based on semiconductor metal-oxides [11] or electrochemical sensing techniques [12,13] have been demonstrated to provide high sensitivity and real-time monitoring. However, their performances are strongly affected by environmental conditions, such as temperature and humidity levels.

Optical sensors represent an effective solution, providing both high sensitivity and high selectivity through laser excitation of gas absorption transitions in the infrared range. Mid-IR Quantum Cascade Lasers (QCLs) combined with multipass cells have been employed for H_2S detection at trace level, demonstrating their applicability for industrial processes aimed at petrochemical environments [14,15]. Chen et al. [16] obtained a minimum detection limit (MDL) of 670 part per billion (ppb) for 2 s averaging time, by means of off-axis integrated cavity output spectroscopy combined with a distributed-feedback (DFB) diode laser emitting around 1.57 μm. A similar telecom fiber-coupled laser and two resonant photoacoustic cells were employed in photoacoustic spectroscopy (PAS) based-systems developed for industrial applications [17,18]. An MDL of 6 ppm was achieved for 10 s integration time [17], whereas long averaging time (~30 min) were required to reach detection limits as low as 500 ppb [18]. PAS basic principle consists in detecting sound waves induced by gas non-radiative energy relaxation as consequence of infrared modulated light absorption. Quartz-enhanced photoacoustic spectroscopy (QEPAS) represents an evolution of the PAS approach and exploits a quartz tuning fork (QTF) to transduce the acoustic wave into an electric signal. The use of QTFs avoids the need for a photodetector, which is mandatory for multipass cells and cavity-based spectroscopy [19]. Reduced dimensions, high sensitivity and fast response time make QEPAS a perfect candidate for realization of compact and portable sensors to be employed for on-site measurements [20–22]. Recently, PAS and QEPAS sensors were developed both for hydrocarbon detection at high concentration or at trace-level [23,24], biomedical applications [25] and detection of dangerous and toxic gases [26,27].

H_2S strongest absorption lies in the THz spectral region. Sampaolo et al. [28] demonstrated a QEPAS sensor for H_2S detection, exploiting a liquid-nitrogen-cooled THz QCL operating in pulsed mode. By targeting a line-strength of $5.53 \bullet 10^{-20}$ cm/mol, an MDL of 2.5 ppm at 300 ms lock-in integration time has been achieved. However, poor quality THz beams, lack of commercially available laser sources, costs and dimensions create serious limits to the implementation of portable sensors. In the Mid-IR spectral range, QCL sources are commercially available with continuous wave output power > 100 mW, but the average absorption linestrength is almost two order of magnitude lower with respect to the THz spectral range [29,30]. Nevertheless, the record in detection limit was achieved in the Mid-IR. Indeed, Helman at al. [29] reached an MDL of 492 ppb for an integration time of 1 s, by exciting a line-strength of $7.77 \cdot 10^{-22}$ cm/mol with an off-beam QEPAS configuration and a continuous wave external cavity QCL (~160 mW optical power). In the Near-IR spectral range, low cost, low weight, and low power consumption DFB diode lasers have been exploited for H_2S detection. An absorption line at 1.57 μm having a linestrength of $1.15 \cdot 10^{-23}$ cm/mol was excited in a QEPAS sensor realized by Kosterev et al. [31] to achieve an MDL of 10 ppm with 35 mW laser power available for PA generation. A sub-ppm MDL was reached employing a similar laser source relying on a erbium-doped fiber amplifier to boost the optical power up to ~1.5 W [32,33]. Viciani et al. [34] achieved a 4 ppm detection limit at 1 s integration time, exploiting a diode laser emitting around 2.6 μm, with an optical power of only 3 mW, but exploiting a line-strength one order of magnitude stronger with respect to the sensor reported in ref [31].

However, none of these research works has ever directly dealt with the main issue afflicting all the H_2S optical sensors. i.e., the almost unavoidable spectral interference between H_2S and CH_4. This problem is absent in the THz range but is a crucial issue when operating in Near-IR and Mid-IR spectral regions. Moreover, for photoacoustic sensing, it is essential to study the response of the sensor system when the gas matrix fluctuates. This requires a detailed analysis of the energetic levels involved in the non-radiative energy relaxation processes to the experimental characterization of the photoacoustic generation and detection. This specific research, focused on H_2S photoacoustic detection in a CH_4-based matrix, has never been carried out as well, so far.

In this work we address these two open issues, demonstrating a Near-IR-QEPAS sensor for H_2S detection providing fast response, high selectivity, and sensitivity. Mixtures of H_2S traces in nitrogen (N_2) or air with CH_4 concentrations up to 1 % were obtained to simulate natural gas leaks dispersed into environment. The influence of CH_4 on H_2S detection in terms of PA generation and interference effect was investigated. Moreover, the employed 2.6 μm DFB laser allowed us to target a Near-IR CH_4 transition as well, with the possibility of achieving a sequential H_2S/CH_4 detection.

2. H_2S and CH_4 relaxation paths

When a gas sample, characterized by a known composition, is dispersed into the environment, the photoacoustic detection of one (or many) molecules within the gas leak requires a detailed investigation of the influence of gas sample matrix, diluted and mixed with the main atmospheric components. The 2.6 μm Near-IR region was identified as spectral-wise suitable for QEPAS detection of H_2S and CH_4. A schematic representation of the infrared energy levels diagram of H_2S, CH_4 and the main atmospheric gas species (N_2, oxygen O_2, and water vapor H_2O) is represented in Fig. 1. For illustration purposes, each spectral band is represented by an energy level placed at the band center. In the region chosen for H_2S/CH_4 excitation, CH_4 spectrum consists of a bending band $3\nu_4$ and a combination band $\nu_2 + 2\nu_4$, creating a cluster of interacting states, i.e. a polyad, at higher energy levels (not shown in the figure) [35]. When one of these states is excited, the vibrational energy is suddenly (in the ns range) transferred to the lower state $3\nu_4$ of the octad. Then, CH_4 relaxation occurs via vibrational to translational (V-T) processes: a bending quantum ν_4 is lost by collisions with the other molecules in their ground states. The overall process is characterized by a collisional rate given by [36]:

$$k_{VT}^{CH_4} = P\sum_i C^i k_{VT}^{CH_4-M_i} \quad (1)$$

where P is the pressure, C^i is the concentration of the collisional partners and $k_{VT}^{CH_4-M_i}$ is the V-T relaxation rate associated to collisions between the excited molecule CH_4^* and the molecule M_i in its ground state. Because of its hydrogen bonds and low moment of inertia, H_2O acts as a V-T relaxation promoter for CH_4. This effect was investigated in several works [37–39]. Moreover H_2O bending mode could be excited via a vibrational-vibrational (V-V) process: the transferred energy is released as kinetic energy for CH_4 PA generation due to the fast H_2O V-T relaxation via self-collisions and collisions with N_2 [40,41]. Similarly, energy relaxation of CH_4 is accompanied by a resonant excitation of O_2 first excited level. However O_2 relaxation rates are much lower than QEPAS modulation frequencies thus the transferred energy is lost for PA generation [42,43].

The V-V processes rate will depend upon the gas pressure and collisional partner concentration M_i according to:

$$k_{VV} = PC^i k_{VV}^{CH_4-M_i} \quad (2)$$

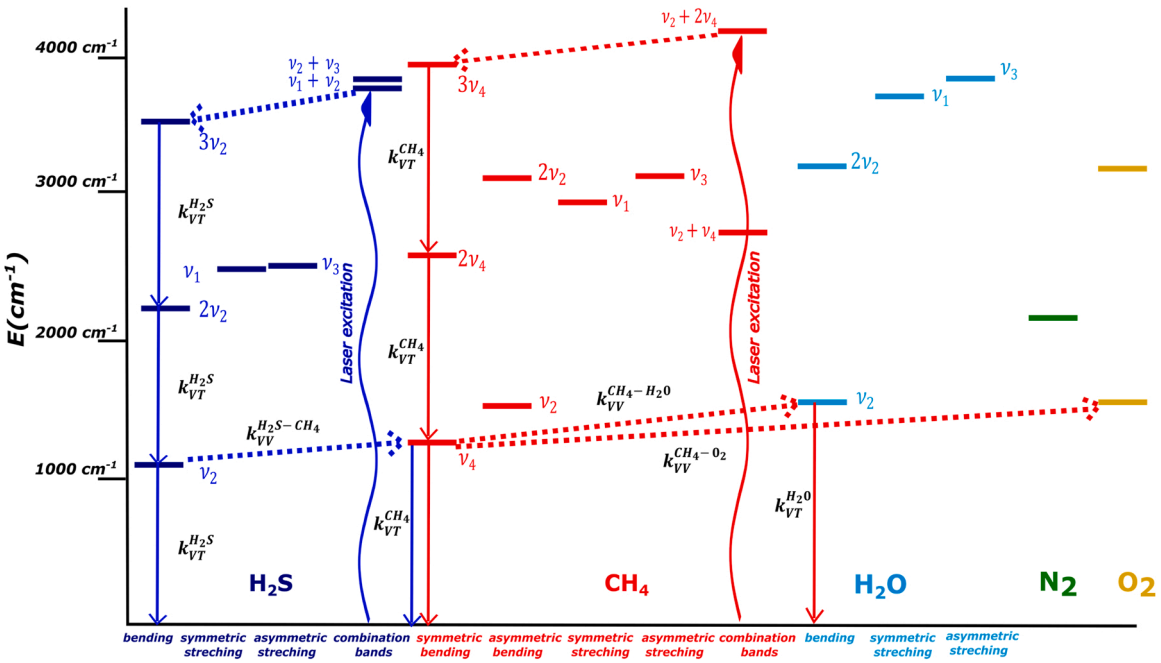

Fig. 1. Energy level diagram showing the laser excitation and the relaxation paths of CH_4 (red arrows) and H_2S (blue arrows) molecules. The red and blue curved arrows are the laser excitations of CH_4 and H_2S energy levels, whereas the solids and dashed arrows represent V-T and V-V processes, respectively. (For interpretation of the references to color in this figure legend, the reader is referred to the web version of this article.)

The V-T and V-V relaxation rates of excited CH_4^* with the main atmospheric components are reported in Table 1.

Analogously H_2S excitation and relaxation are examined. H_2S spectra is characterized by a triad composed of the bending mode $3\nu_2$ and two combination bands ($\nu_1 + \nu_2$, $\nu_2 + \nu_3$) [44,45]. However, to our knowledge, no studies reporting on H_2S V-V and V-T relaxation paths and the associated collisional rates are available in literature, so far. Nonetheless the following hypothesis could be done:

- Laser excitation of one of H_2S states of the triad is followed by energy transfer to $3\nu_2$ band, which is the lowest state of the triad. H_2S V-T relaxation results in the loss of the lowest energy quantum ν_2 and can be described by a formula similar to Eq. (1).
- H_2S shows similar vibrational de-excitation velocity compared to H_2O due to their similar chemical properties. Thus, the effects of H_2O as a V-T promoter for H_2S relaxation should be almost negligible [46]. Indeed, Viciani et al. [34] observed this effect in the 2.6 μm Near-IR spectral region for up to 2 % H_2O concentration.
- A V-V exchange is energetically possible between $H_2S^*(\nu_2)$ and CH_4 since the energy difference ($\Delta\nu = 128\ cm^{-1}$) is less than the thermal energy ($k_BT \sim 207\ cm^{-1}$) [47]. V-V exchanges with other molecules are unlikely due to higher energy gap between the involved vibrational bands.

Table 1
V-T relaxation rates of the n^{th} CH_4 vibrational state with the main collisional partners in standard air. The reactions in bold represent the V-V processes.

	k ($s^{-1}Torr^{-1}$)	Ref
$CH_4^*(n\nu_4) + CH_4 \rightarrow CH_4^*((n-1)\nu_4) + CH_4$	$1.32*10^3$	[42]
$CH_4^*(n\nu_4) + H_2O \rightarrow CH_4^*((n-1)\nu_4) + H_20$	$1.05*10^5$	[37]
$CH_4^*(n\nu_4) + N_2 \rightarrow CH_4^*((n-1)\nu_4) + N_2$	$1.32*10^5$	[42]
$CH_4^*(n\nu_4) + O_2 \rightarrow CH_4^*((n-1)\nu_4) + O_2$	$1.71*10^3$	[42]
$\mathbf{CH_4^*(\nu_4) + O_2 \rightarrow CH_4 + O_2^*}$	$\mathbf{4.34*10^3}$	[43]
$\mathbf{CH_4^*(\nu_4) + H_2O \rightarrow CH_4 + H_2O^*(\nu_2)}$	$\mathbf{2.60*10^4}$	[40]

3. Experimental apparatus

The schematic of the experimental setup is shown in Fig. 2.

The laser source is a DFB diode laser emitting around 2638 nm with an output power up to 12 mW. A thermoelectric cooler (TEC) and a current driver (CD) allow setting the laser temperature and providing current for the laser diode, respectively. The laser light is focused through an acoustic detection module (ADM) by means of a plano-convex Si lens, with a focal length of 75 mm. The ADM consists of a gas cell equipped with an inlet and an outlet window, allowing the gas mixture to flow through the airtight chamber containing a spectrophone, composed of a T-shaped QTF and in-plane acoustic resonator (AR) tubes [48]. The spectrophone has a resonance frequency $f_0 = 12,458.52$ Hz and quality factor $Q = 32,140$ at $P = 100$ Torr in a mixture containing pure N_2. A voltage ramp and a sinusoidal dither are applied to the laser source to finely tune the laser emission wavelength and modulate the laser light at the half of the QTF fundamental resonance mode $f_0/2$, respectively. Both signals are provided by a TEKTRONIC AFG 31,000 waveform generator. The piezoelectric current was converted into an electrical signal by a transimpedance amplifier (TA) and the f_0 component was detected by a lock-in amplifier (2 f-Wavelength Modulation). A data acquisition card (National Instrument USB 6361) and a LabVIEW-based software are used to acquire the demodulated signal. The gas handling system is composed of an MCQ Instrument Gas Blender GB-100, used to manage the flow rate for three gas channels and produce the desired gas mixture. Pure N_2 was used as carrier gas. A Nafion humidifier (PermSelect PDMSXA) was placed downstream the gas mixer to humidify the samples (not shown in the figure), fixing the H_2O concentration for all measurements at 1 % of absolute humidity. Relative humidity and temperature within the gas line were measured by an IST AG HYT 271 sensor positioned near the ADM (not shown in the figure). An MKS type 649 pressure controller/flow meter, in combination with a needle valve and a pump allowed fixing the gas pressure and monitoring the flow rate inside the gas line. The gas flow rate was fixed at 50 sccm, with a 1 % of accuracy of the flow setpoint of each channel provided by the instrument datasheet.

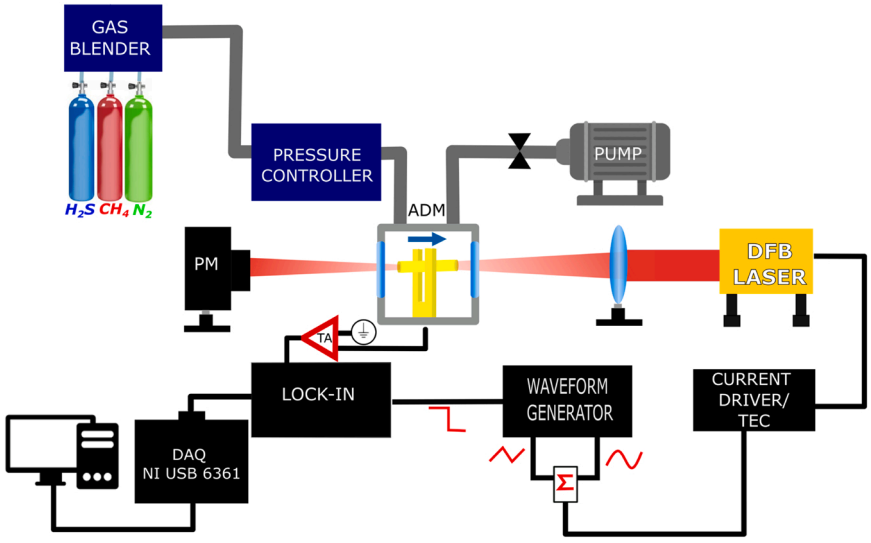

Fig. 2. Schematic of the experimental apparatus. ADM-acoustic detection module, DFB- distributed feedback laser, TEC-thermoelectric cooler, PM-power meter.

4. Sensor performance for H_2S and CH_4 detection

4.1. Preliminary characterization

By tuning the laser temperature, the Near-IR spectral region from 3788 cm^{-1} to 3795 cm^{-1} can be investigated. With the aim of pursuing a sequential detection of CH_4 and H_2S, the detection scheme requires the laser temperature to be set at T = 20 °C to excite the CH_4 absorption line located at 3791.67 cm^{-1}, with a line strength of $4.41 \cdot 10^{-26}$ cm/molecule for 1000 ppm of CH_4. Then, the laser temperature is set at T = 15 °C to target the H_2S absorption line at 3793.24 cm^{-1} with a line strength of $1.47 \cdot 10^{-26}$ cm/molecule for 10 ppm of H_2S [49]. The optical power available for PA generation, in correspondence of both the absorption lines selected, was measured to be ~ 7 mW. QEPAS sensor response was also studied in terms of gas pressure and modulation amplitude and optimized for H_2S detection.

Fig. 3a reports the H_2S QEPAS peak signal as a function of the gas pressure for a gas target concentration of 150 ppm diluted in N_2. The pressure maximizing H_2S QEPAS signal was experimentally found to be 200 Torr. In Fig. 3b, a comparison between QEPAS spectra of a mixture composed of 150 ppm H_2S in N_2 acquired at 100 Torr and 200 Torr, respectively, with 100 ms integration time, are shown.

It can be easily noted that at 200 Torr, a non-zero background absorption arises with respect to the noise level at 100 Torr. This is due to the interference of a nearby absorption line of H_2O. This effect is levelled off at P = 100 Torr, with only a ~ 10 % loss in the QEPAS signal. As a result, all measurements for both analytes were carried out at P = 100 Torr, with an optimum amplitude modulation of 20 mV. HITRAN database was used to simulate the absorption cross section of CH_4-based gas leak, containing H_2S, dispersed in air and analyzed at a pressure of 100 Torr. The simulated spectrum, shown in Fig. 4, is related to 1000 ppm of CH_4 and 10 ppm of H_2S, mixed with a standard air mixture containing typically 1.19 % H_2O, 20.90 % O_2, 77.87 % N_2 and traces of other gases [49].

The simulation clearly shows the spectral scenario to deal with: at 100 Torr, H_2S and CH_4 do not interfere each other and H_2O is the only absorber potentially interfering with the two target molecules. Once experimentally verified that, at the selected operating pressure, the pressure broadening of the H_2O line at 3792.6 cm^{-1} (Fig. 4, upper panel) is small enough to not influence the H_2S signal background, the possible H_2O interference on CH_4 detection must now be excluded. Thereby, it was verified that almost all the nearby H_2O lines were under the sensitivity of our QEPAS sensor. The only detectable H_2O absorption feature at 3791.8 cm^{-1} did not affect CH_4 line shape at the selected

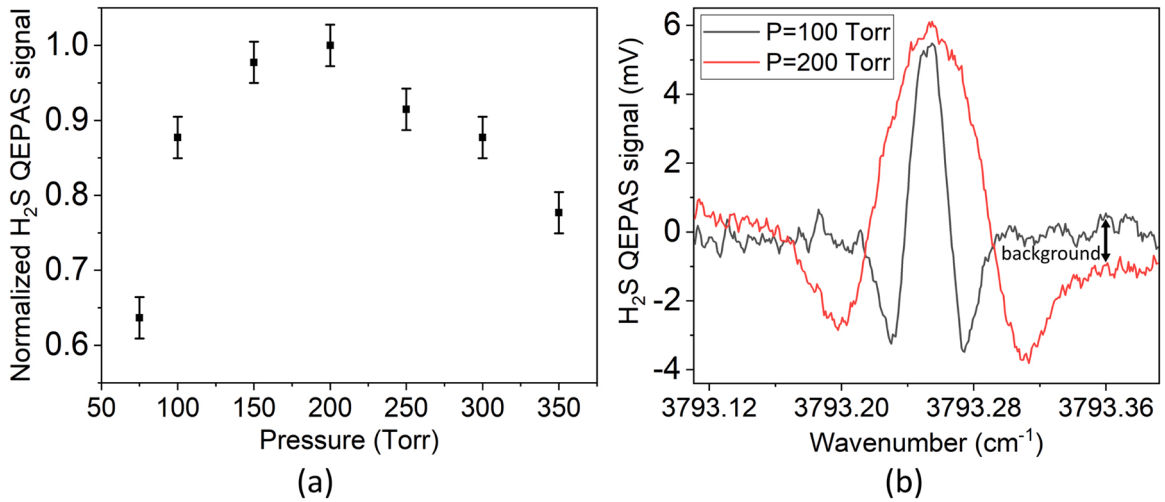

Fig. 3. a) Normalized H_2S QEPAS peak signal as a function of gas pressure. The data refer to a gas mixture of 150 ppm of H_2S in N_2. b) Spectra of 150 ppm of H_2S in N_2 recorded at 100 Torr and 200 Torr at 100 ms integration time. The non-zero background absorption at P = 200 Torr is marked by the black arrow.

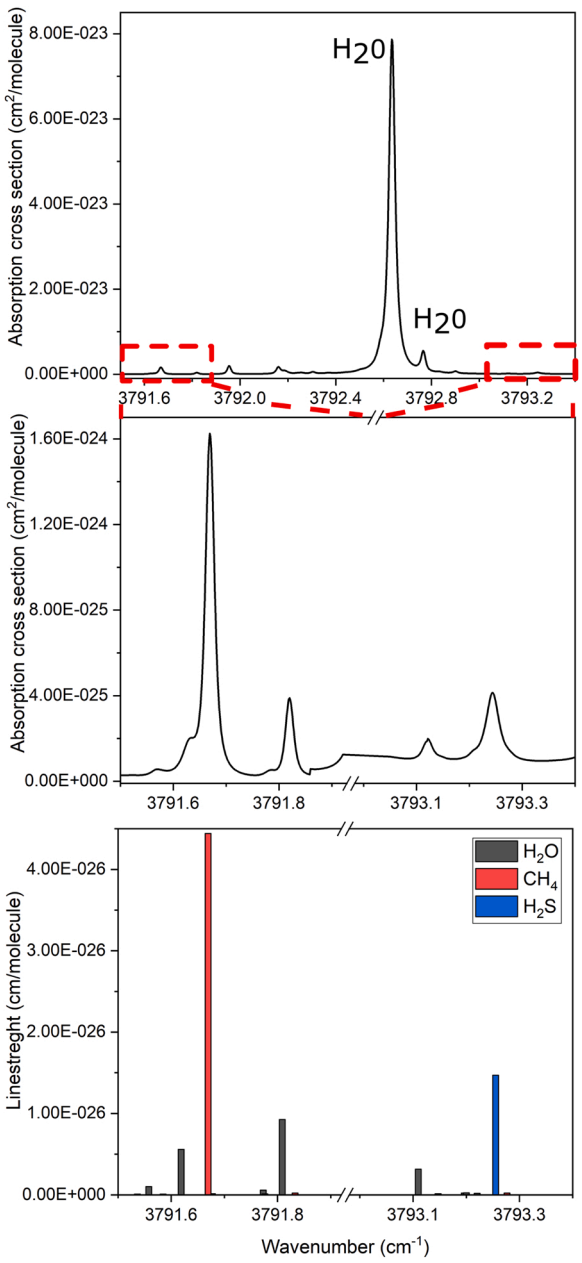

Fig. 4. Absorption cross section of a mixture of 10 ppm of H_2S, 1000 ppm of CH_4 and air (1.19 % H_2O, 20.90 % O_2, 77.87 % N_2 and traces of other gases) at P = 100 Torr and T = 296 K. Upper panel: simulation in the spectral region 3791.5–3793.4 cm^{-1}. Central panel: enlarged view around the selected H_2S and CH_4 absorption lines. Lower panel: stick spectrum of H_2O, H_2S and CH_4 analytes in the same ranges of the central panel.

working pressure.

Following these preliminary characterizations, the most appropriate integration time τ for sensor calibration was chosen. Based on a possible further development and engineering of this QEPAS prototype as H_2S in-situ and real-time leak detector, a trade-off must be found between fast-response time and high sensitivity. We experimentally verified that 2 s integration time and 4 s acquisition time allowed us to unambiguously detect H_2S QEPAS signal with respect to noise level in the few ppm scale, providing a signal to noise ratio (SNR) of ~ 4 for a 10 ppm H_2S concentration in N_2, as it will be demonstrated in the following section.

4.2. H_2S and CH_4 calibration in N_2

Firstly, the sensor calibration for H_2S and CH_4 detection was carried out in a concentration range typical of a CH_4-based leak containing H_2S, dispersed into the environment. CH_4 concentration was varied from 0.03 % to 1 % using a certified mixture of 1 % CH_4 in N_2 and N_2 as carrier gas. Similarly, we analyzed the QEPAS response for H_2S detection from 10 ppm to 250 ppm using a certified mixture of 250 ppm of H_2S in N_2. The calibration curves, consisting in the 2 f-QEPAS signal peak values acquired at different concentrations, with a 2 s integration time, are shown in Fig. 5. A linear trend was verified for both analytes with a linearity coefficient of 0.0368 mV/ppm and 0.0011 mV/ppm for H_2S and CH_4, respectively.

In order to investigate how the detection limits of the sensor improve as a function of the integration time, an Allan-Werle deviation analysis of H_2S QEPAS signal was performed [50]. A 2-hour long acquisition (0.1 s lock-in integration time and 0.3 s acquisition time) was carried out in N_2 at P = 100 Torr and at a laser current fixed far from gas absorption. The results are shown in Fig. 6: MDL is plotted as a function of integration time starting from 2 s integration time with MDL equal to 2.5 ppm. The NNEA for H_2S detection was found equal to 8.8 * 10^{-9} $cm^{-1}W/Hz^{1/2}$. H_2S detection limit can be further improved to the sub-ppm scale by increasing the integration time up to 30 s, but such sensitivity and response time levels are not functional for real time detection. *By performing a similiar analysis for CH_4, a MDL of 85 ppm was calculated for a 2 s integration time.*

4.3. Influence of CH_4 on H_2S detection

The sensor performances for detection of both analytes in the same mixture were analyzed. In Fig. 7, the measured QEPAS signal for a N_2-based mixture of 1 % CH_4 and 125 ppm H_2S, obtained diluting a 10 % certified concentration, is compared to the QEPAS spectrum of the single analytes diluted in N_2.

It is evident that H_2S traces do not influence the CH_4 QEPAS signal neither in terms of interference effect nor as a V-T promoter. Conversely, a ~ 38 % reduction of the H_2S peak signal was observed when increasing the CH_4 concentration in the mixture from 0 % to 1 %. When a spectrophone is employed in a QEPAS sensor for gas detection, several factors can affect the detection of a given target molecule, such as H_2S in this case [51].

4.3.1. Influence of gas density on QTF resonance properties

QTF quality factor was measured by electrically exciting the QTF around the expected resonance frequency. By performing a Lorentzian fit, the QTF quality factor measured for a mixture composed of 1 % CH_4 and 125 ppm H_2S in N_2 was found equal to 32,933, differing by less than ~3 % with respect to the Q measured with no CH_4 in the mixture (32,140). This difference is also lower than the uncertainty on Q-factor value calculated from the fitting errors. Thereby this effect can be also neglected. These variations in the matrix composition didn't affect the resonance frequency as well, shifting from 12,458.54 Hz to 12,458.52 Hz. The experimental results were also compared to theoretical calculations. The Q-factor related to fluid damping can be derived by the model developed by Hosaka et al. which is an approximation for vibrating rectangular prongs oscillating in a viscous gas matrix [52]. The applicability of this model to QTFs vibrating at the fundamental and overtone mode was experimentally demonstrated [53,54]. In addition, the model was validated for T-shaped QTFs, like the one employed in this work [55]. Based on this model, the damping contribute to the overall quality factor can be theoretically evaluated as follows:

$$Q_{gas} = \frac{4\rho T w^2 f_o}{3\mu_{gas} w + \frac{3}{4} w^2 \sqrt{(4\pi\rho_{gas}\,\mu_{gas} f_o)}} \quad (3)$$

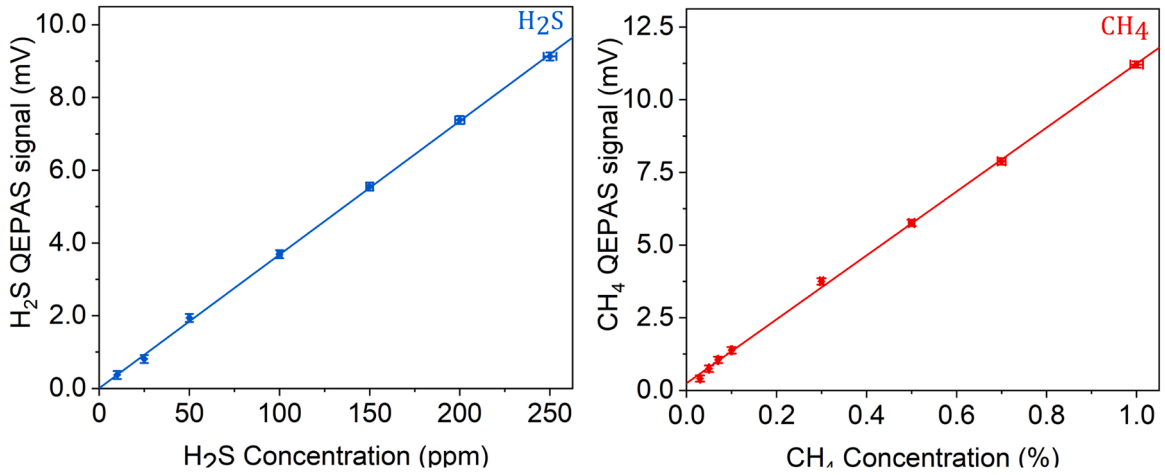

Fig. 5. QEPAS peak signal versus CH_4 (left panel) and H_2S (right panel) concentration acquired at 2 s integration time and P = 100 Torr. The solid lines represent the best linear fits.

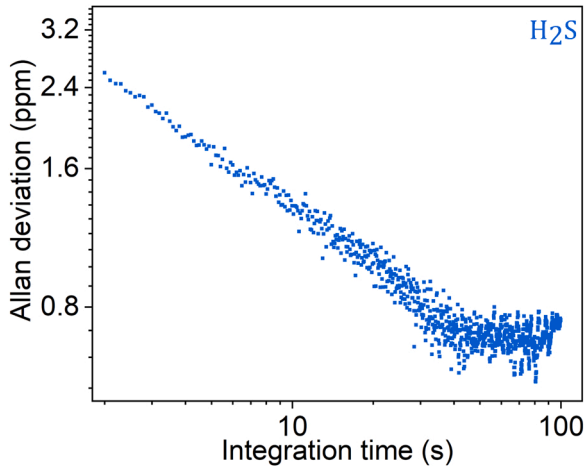

Fig. 6. Allan deviation of H_2S QEPAS signal as a function of integration time. At 2 s integration time, the calculated MDL is 2.5 ppm.

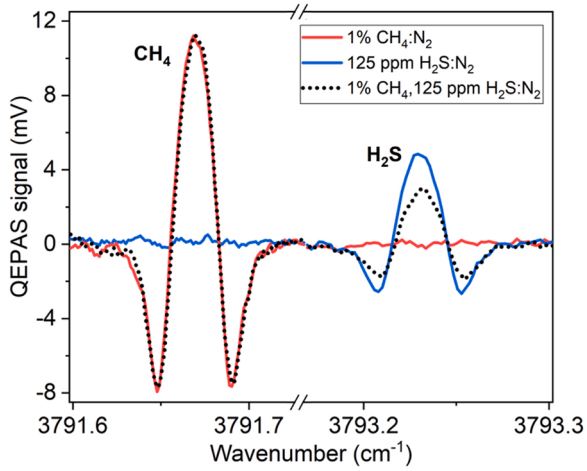

Fig. 7. 2 f CH_4 and H_2S QEPAS spectra measured for three mixtures: 1 % CH_4 in N_2,125 ppm H_2S in N_2 and 1 % CH_4 and 125 ppm H_2S in N_2.

where $f_o = 12458.52$Hz is the QTF resonance frequency, w = 0.25mm is the crystal width, T = 1.4mm is the prong thickness and $\rho = 2650$ kg/m^3 is the quartz density. $\rho_{gas} = M_{gas}\,P/RT$ and μ_{gas} are the gas density and the dynamic viscosity of the mixture, respectively. Both M_{gas} and μ_{gas} are calculated as a sum of each gas species molar mass and viscosity, respectively, weighted by their concentration. By using Eq. (3) it can be evaluated that a Q_{gas}variation larger than 3 % is obtained for CH_4 concentrations higher than 8 %, which is well above the typical concentration range for leaks detection.

4.3.2. *Influence of sound speed on AR tubes' signal enhancement*

Gas mixture composition could modify the speed of sound, causing a detuning between acoustic resonance of the resonator tubes and that of the QTF. Indeed, the effective tube length for the fundamental resonance mode of resonator tubes depends upon the sound velocity v_s according to [56]:

$$l = \frac{v_s}{2f_o} - \frac{16d}{3\pi} \tag{4}$$

where f_0 is the QTF fundamental resonance frequency and d is the internal tubes diameter (1.59 mm). Evaluating v_s through the ideal gas sound velocity [31] a negligible variation of ~ 26 μm in the optimum tube length was calculated when increasing the CH_4 concentration in the mixture from 0 % to 1 %. Significant decreases in the QEPAS peak signal has been observed only for tube length variations larger than 1 mm with respect to the optimal tube length [48]. Thereby also in this case the effect on the QEPAS signal is negligible.

4.3.3. *CH_4 influence on H_2S relaxation dynamics*

It remains one last effect to investigate, i.e., the V-V energy transfer (see Fig. 1) from H_2S to CH_4 molecules, which can negatively affect the H_2S photoacoustic generation due to a retarded energy relaxation. We extended the CH_4 concentration range up to 5 %, to investigate the influence of the matrix effect on H_2S relaxation. Based on the previous calculations, the acoustic QTF response was considered flat for all the investigated mixtures. This was also confirmed experimentally. The QEPAS peak signals measured for 50 ppm (red dots),100 ppm (blue dots) and 125 ppm (black dots) H_2S concentrations are plotted as a function of CH_4 concentration in Fig. 8a. H_2S signal was experimentally found to be not affected by CH_4 contamination in the carrier gas up to 0.1 % concentration. This is clear from the inset of Fig. 8a, where the fluctuation of the H_2S peak signal mean value over 4 acquisitions, observed in the range 0.03–0.01 %, fall within the 1-σ noise error bars calculated for each CH_4 concentration (0.1 mV). This is also confirmed

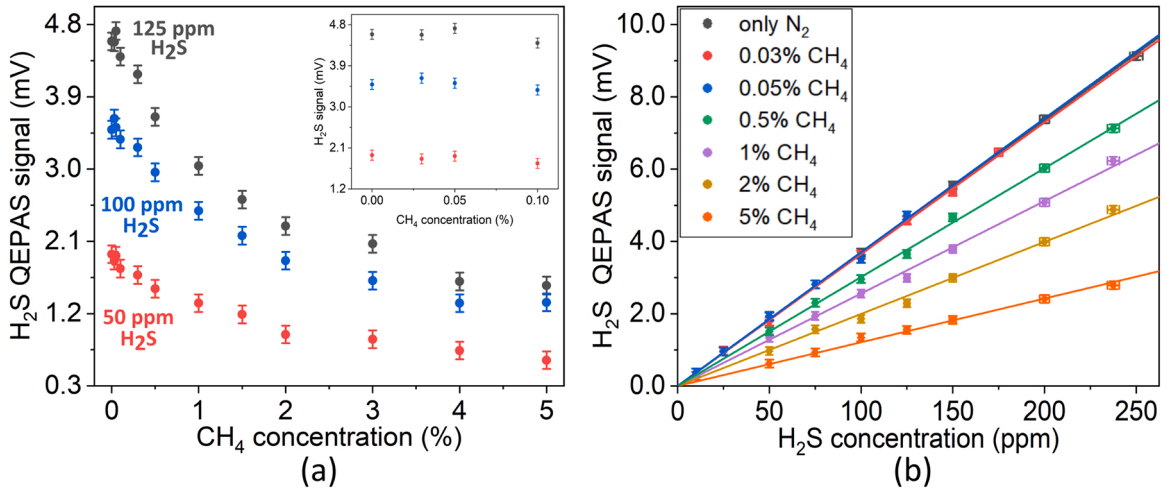

Fig. 8. (a) H_2S QEPAS signal as a function of CH_4 concentration. The data refer to H_2S concentrations of 50 ppm (red dots), 100 ppm (blue dots) and 125 ppm (black dots). The inset shows an enlarged view in the 0.03–0.1 % range of CH_4 concentration (b) H_2S calibration in mixtures containing both CH_4 and N_2. (For interpretation of the references to color in this figure legend, the reader is referred to the web version of this article.)

by comparing in Fig. 7b the nearly perfect overlap between the H_2S calibration curves obtained in N_2 with those measured for mixtures containing CH_4 concentrations of 300 ppm and 500 ppm. The linear fit coefficients, their uncertainty and the calculated MDLs are reported in Table 2. Thereby, the obtained results demonstrate that the presence of CH_4 molecules up to per thousand range in the N_2-based matrix do not significantly modify the H_2S V-T relaxation rate, which thus occurs primarily thorough collisions with gas components at tens of per cents concentration, namely N_2.

As CH_4 concentration increases above the per thousand scale, H_2S QEPAS signal drops down reaching a plateau for concentrations > 4 %, corresponding to a peak value reduction of ~ 70 %. Exponential decrease of PAS signal cannot be explained by simply assuming V-T relaxation but are clear evidence of the presence of V-V processes resulting in energy transfer to slower relaxation channels [42,57,58]. Based on the discussion presented in the first section, a V-V exchange from H_2S^* (ν_2) to CH_4 is likely to happen due to their similar energy. If CH_4 concentration is sufficiently high, the rate associated with this process given by $C_{CH_4} Pk_{VV}^{H_2S-CH_4}$, becomes comparable to the rate characterizing the V-T process $k_{VT}^{H_2S}$(see Eq. (1)). However, the vibrational energy transferred to CH_4 molecules is not efficiently converted into translational energy, and thus available for photoacoustic generation, due to CH_4 slow relaxation times with respect to water-like molecules, such as H_2S. The observed plateau corresponds to a saturation of the number of collisions occurring between H_2S and CH_4.

In principle, a phase shift should be directly related to the above-mentioned V-T, V-V processes. [42,57,58]. Nevertheless, the relatively low operating pressure of 100 Torr used for all the measurements didn't allow an unambiguous interpretation of the phase data. In fact, the phase shift in the photoacoustic signal can be calculated as $\Phi(\tau) = \arctan(2\pi f\tau)$, where f is the modulation frequency and τ is the non-radiative relaxation time. Provided that $\tau^{-1} = P\sum_i C_i k_i$ [42], the capability of the system in recognizing phase shifts due to variations in concentration of the collisional partners strongly decreases at lower pressures, where the slope of the $\Phi(\tau)$ function is lower as well.

From this investigation, it follows that the H_2S calibration curve must be necessarily adapted to the CH_4 concentration to properly interpret the QEPAS signals and accurately retrieve the H_2S concentration, when the CH_4 component in the gas matrix exceeds 1000 ppm.

Thereby, several calibration curves have been extracted for different CH_4 concentration, up to 5 % and the obtained results are reported in Fig. 8b and Table 2. An H_2S sensor MDL lower than 4 ppm was calculated for CH_4 concentration up to 1 % and worsens to ~ 8 ppm for 5 % CH_4 concentration, where CH_4 quenching effect is saturated. It is worth to notice that the obtained detection limits at 2 s integration time are below the OHSA's long exposure limit.

The applicability of H_2S/CH_4 detection in a standard air matrix was also investigated. With this purpose, we acquired QEPAS spectra for mixtures obtained by replacing N_2 with standard air (20 % O_2, 1 % H_2O and 79 % N_2) as carrier gas. Fig. 9 shows a comparison between the spectra obtained for a mixture of 1000 ppm of CH_4 and 50 ppm of H_2S diluted in N_2 and in standard air, respectively. A 30 % reduction of the

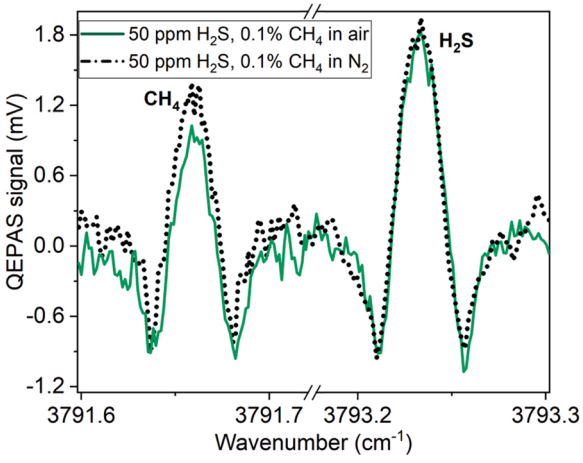

Fig. 9. 2 f CH_4 and H_2S QEPAS spectra measured for two mixtures: 50 ppm H_2S, 0.1 % CH_4 and N_2. 50 ppm H_2S, 0.1 % CH_4 and air.

Table 2
Slopes and MDL of H_2S calibrations obtained by using mixtures of N_2 and CH_4 as carrier gas.

	Only N_2	0.03 % CH_4	0.05 % CH_4	0.5 % CH_4	1 % CH_4	2 % CH_4	5 % CH_4
Slope (mV/ppm)	0.0368 ± 0.0001	0.0365 ± 0.0003	0.0370 ± 0.0005	0.0301 ± 0.0002	0.0256 ± 0.0003	0.0199 ± 0.0003	0.0121 ± 0.0002
MDL (ppm)	2.5	2.5	2.5	3	3.7	4.7	7.8

CH_4 QEPAS signal was observed. This experimental evidence, together with the resonance properties of the resonator remaining unchanged also in standard air, points in the direction of a V-V exchange occurring between excited CH_4 and O_2 molecules, as explained in the first section. The energy transferred to O_2 is thus expected to be substantially lost due to the slow V-T relaxation time (0.63 ms) compared to one period of laser modulation (0.08 ms) resulting in a lower CH_4 signal. Consequently, CH_4 signal interpretation should take into account the presence of O_2 and of the fluctuations in H_2O concentration [58]. On the contrary, H_2S peak remained unaffected by the matrix variation, showing that no efficient V-T or V-V exchange can occur with O_2 molecules, neither with H_2O. Thus, the calibrations obtained for H_2S detection in a matrix containing CH_4 up to per thousands, H_2O ($\sim$ 1 %) and N_2 are still valid when the gas matrix is represented by standard air, since O_2 at the $\sim$ 20 % level does not affect the photoacoustic generation.

5. Conclusions

We presented a Near-IR-QEPAS sensor capable of a fast-response sensing of H_2S trace-gas, within a matrix containing N_2 and CH_4 up to few percent. Spectral window of operation and detection parameters, such as gas sample pressure and modulation amplitude, were identified in order to avoid spectral interference among H_2O, CH_4 and H_2S absorption lines. The high selectivity provided by the sensing system allowed us to focus on the analysis of H_2S photoacoustic detection nonlinearities arising from the interaction with the gas matrix. Firstly, the complete scheme of the energy levels involved was evaluated to qualitatively identify the possible pattern of V-T and V-V energy transfers. Then, a systematic characterization of the H_2S signal cross-correlations with other components was carried out. Indeed, we demonstrated that V-V energy transfer from H_2S to CH_4 for CH_4 concentrations larger than 1000 ppm degrades H_2S QEPAS signal. Nonetheless, we demonstrated that the sensor detection limit for H_2S detection at 2 s integration time was well below the OHSA's long exposure limit (20 ppm) in all the investigated gas matrices. MDL was calculated as low as 4 ppm for CH_4 concentration $\leq$ 1 % in the matrix, which can be assumed as a reasonable reference concentration representing relatively small natural gas leaks dispersed into environment. We validated the sensor for H_2S detection in a standard air-based matrix, demonstrating the sensor potentiality for on-field and real-time measurements deployment.

As a future development of this experimental investigation, the presented measurements can be repeated at higher pressures to obtain a more reliable evaluation of the QEPAS signal phase shifts and pursue a complete characterization of H_2S relaxation processes. This type of measurements should require the employment of higher H_2S concentrations to increase QEPAS SNR and compensate both for background absorption interference arising from the broadening of CH_4 and H_2O features, and for Q-factor deterioration.

In addition, our sensor performance, together with the commercial availability of Near-IR sources, demonstrate its applicability for realizing portable safety sensors detecting CH_4 and H_2S emissions from natural gas reservoirs or in industrial areas. For this future development, a line-locking configuration will be implemented, rather than full spectral scan acquisitions: H_2S peak signal would be continuously monitored and, when a non-zero signal indicating a leak arises, the system would send alerts and sequentially look for CH_4 concentration to i) compensate the H_2S signal and accurately retrieve its concentration, if needed, ii) evaluate the fire/explosion potential due to the leak. In addition, a future development will be engineering this QEPAS prototype in an explosion proof sensor deployable for in situ leak detection.

Declaration of Competing Interest

The authors declare the following financial interests/personal relationships which may be considered as potential competing interests: Angelo Sampaolo reports equipment, drugs, or supplies and travel were provided by Polytechnic University of Bari.

Data availability

Data will be made available on request.

Acknowledgements

The project was sponsored by the National Key R&D Program of China (No. 2019YFE0118200); the European Union's Horizon 2020 Research and Innovation Program under grant agreement (No. 101016956 PASSEPARTOUT); National Natural Science Foundation of China (NSFC) (Nos. 62175137, 62075119 and 61805132); Shanxi Science Fund for Distinguished Young Scholars (No. 20210302121003).

References

[1] Occupational Safety and Health Administration, (n.d.). https://www.osha.gov/.
[2] T.L. Guidotti, Hydrogen sulfide: advances in understanding human toxicity, Int. J. Toxicol. 29 (2010) 569–581, https://doi.org/10.1177/1091581810384882.
[3] M. Drimal, K. Koppová, Z. Klöslová, E. Fabiánová, Environmental exposure to hydrogen sulfide in central Slovakia (Ružomberok area) in context of health risk assessment, Cent. Eur. J. Public Health 18 (2010) 224–229, https://doi.org/10.21101/cejph.a3610.
[4] J. Aali, H. Rahimpour-Bonab, M.R. Kamali, Geochemistry and origin of the world's largest gas field from Persian Gulf, Iran, J. Pet. Sci. Eng. 50 (2006) 161–175, https://doi.org/10.1016/j.petrol.2005.12.004.
[5] K. El Hachem, M. Kang, Methane and hydrogen sulfide emissions from abandoned, active, and marginally producing oil and gas wells in Ontario, Canada, Sci. Total Environ. 823 (2022), https://doi.org/10.1016/J.SCITOTENV.2022.153491.
[6] N. Gasunie, Eleventh Report of the European Gas Pipeline Incident Data Group (Period 1970–2019), (2020). ⟨https://www.egig.eu/reports⟩.
[7] G.C.A. Schuit, B.C. Gates, Chemistry and engineering of catalytic hydrodesulfurization, AIChE J. 19 (1973) 417–438, https://doi.org/10.1002/AIC.690190303.
[8] M.N. Bates, N. Garrett, P. Shoemack, Investigation of health effects of hydrogen sulfide from a geothermal source, Arch. Environ. Health 57 (2002) 405–411, https://doi.org/10.1080/00039890209601428.
[9] M.S. Legator, D.L. Morris, D.L. Philips, C.R. Singleton, Health effects from chronic low-level exposure to hydrogen sulfide, Arch. Environ. Health 56 (2001) 123–131, https://doi.org/10.1080/00039890109604063.
[10] S.K. Pandey, K.H. Kim, A review of methods for the determination of reduced sulfur compounds (RSCS) in air, Environ. Sci. Technol. 43 (2009) 3020–3029, https://doi.org/10.1021/ES803272F.
[11] G. Fang, Z. Liu, C. Liu, K. lun Yao, Room temperature H2S sensing properties and mechanism of CeO2-SnO2 sol-gel thin films, Sens. Actuators B Chem. 66 (2000) 46–48, https://doi.org/10.1016/S0925-4005(99)00467-0.
[12] C. Yu, Y. Wang, K. Hua, W. Xing, T. Lu, Electrochemical H2S sensor with H2SO4 pre-treated Nafion membrane as solid polymer electrolyte, Sens. Actuators B Chem. 86 (2002) 259–265, https://doi.org/10.1016/S0925-4005(02)00200-9.
[13] N.S. Lawrence, J. Davis, L. Jiang, T.G.J. Jones, S.N. Davies, R.G. Compton, The electrochemical analog of the methylene blue reaction: a novel amperometric approach to the detection of hydrogen sulfide, Electroanalysis 12 (2000) 1453–1460, https://doi.org/10.1002/1521-4109(200012)12:18<1453::AID-ELAN1453>3.0.CO;2-Z.
[14] H. Moser, W. Pölz, J.P. Waclawek, J. Ofner, B. Lendl, Implementation of a quantum cascade laser-based gas sensor prototype for sub-ppmv H2S measurements in a petrochemical process gas stream, Anal. Bioanal. Chem. 409 (2017) 729–739, https://doi.org/10.1007/s00216-016-9923-z.
[15] M. Nikodem, K. Krzempek, D. Stachowiak, G. Wysocki, Quantum cascade laser-based analyzer for hydrogen sulfide detection at sub-parts-per-million levels, Opt. Eng. 57 (2017) 1, https://doi.org/10.1117/1.oe.57.1.011019.
[16] W. Chen, A.A. Kosterev, F.K. Tittel, X. Gao, W. Zhao, H2S trace concentration measurements using off-axis integrated cavity output spectroscopy in the near-infrared, Appl. Phys. B Lasers Opt. 90 (2008) 311–315, https://doi.org/10.1007/s00340-007-2858-5.
[17] A. Szabó, Á. Mohácsi, G. Gulyás, Z. Bozóki, G. Szabó, In situ and wide range quantification of hydrogen sulfide in industrial gases by means of photoacoustic spectroscopy, Meas. Sci. Technol. 24 (2013), https://doi.org/10.1088/0957-0233/24/6/065501.
[18] A. Varga, Z. Bozóki, M. Szakáll, G. Szabó, Photoacoustic system for on-line process monitoring of hydrogen sulfide (H2S) concentration in natural gas streams, Appl. Phys. B Lasers Opt. 85 (2006) 315–321, https://doi.org/10.1007/s00340-006-2388-6.
[19] P. Patimisco, G. Scamarcio, F.K. Tittel, V. Spagnolo, Quartz-enhanced photoacoustic spectroscopy: a review, Sensors 14 (2014) 6165–6206, https://doi.org/10.3390/s140406165.
[20] A. Sampaolo, S. Csutak, P. Patimisco, M. Giglio, G. Menduni, V. Passaro, F.K. Tittel, M. Deffenbaugh, V. Spagnolo, Methane, ethane and propane detection using a compact quartz enhanced photoacoustic sensor and a single interband cascade

laser, Sens. Actuators B Chem. 282 (2019) 952–960, https://doi.org/10.1016/j.snb.2018.11.132.
[21] A. Sampaolo, G. Menduni, P. Patimisco, M. Giglio, V.M.N. Passaro, L. Dong, H. Wu, F.K. Tittel, V. Spagnolo, Quartz-enhanced photoacoustic spectroscopy for hydrocarbon trace gas detection and petroleum exploration, Fuel 277 (2020), 118118, https://doi.org/10.1016/j.fuel.2020.118118.
[22] F. Sgobba, A. Sampaolo, P. Patimisco, M. Giglio, G. Menduni, A.C. Ranieri, C. Hoelzl, H. Rossmadl, C. Brehm, V. Mackowiak, D. Assante, E. Ranieri, V. Spagnolo, Compact and portable quartz-enhanced photoacoustic spectroscopy sensor for carbon monoxide environmental monitoring in urban areas, Photoacoustics 25 (2022), 100318, https://doi.org/10.1016/j.pacs.2021.100318.
[23] G. Menduni, A. Zifarelli, A. Sampaolo, P. Patimisco, M. Giglio, N. Amoroso, H. Wu, L. Dong, R. Bellotti, V. Spagnolo, High-concentration methane and ethane QEPAS detection employing partial least squares regression to filter out energy relaxation dependence on gas matrix composition, Photoacoustics 26 (2022), 100349, https://doi.org/10.1016/j.pacs.2022.100349.
[24] H. Xiao, J. Zhao, C. Sima, P. Lu, Y. Long, Y. Ai, W. Zhang, Y. Pan, J. Zhang, D. Liu, Ultra-sensitive ppb-level methane detection based on NIR all-optical photoacoustic spectroscopy by using differential fiber-optic microphones with gold-chromium composite nanomembrane, Photoacoustics 26 (2022), 25100353, https://doi.org/10.1016/J.PACS.2022.100353.
[25] Z. Shang, S. Li, B. Li, H. Wu, A. Sampaolo, P. Patimisco, V. Spagnolo, L. Dong, Quartz-enhanced photoacoustic NH3 sensor exploiting a large-prong-spacing quartz tuning fork and an optical fiber amplifier for biomedical applications, Photoacoustics 26 (2022), 100363.
[26] X. Liu, S. Qiao, G. Han, J. Liang, Y. Ma, Highly sensitive HF detection based on absorption enhanced light-induced thermoelastic spectroscopy with a quartz tuning fork of receive and shallow neural network fitting, Photoacoustics 28 (2022), 100422, https://doi.org/10.1016/J.PACS.2022.100422.
[27] S. Qiao, A. Sampaolo, P. Patimisco, V. Spagnolo, Y. Ma, Ultra-highly sensitive HCl-LITES sensor based on a low-frequency quartz tuning fork and a fiber-coupled multi-pass cell, Photoacoustics 27 (2022), 100381, https://doi.org/10.1016/J.PACS.2022.100381.
[28] A. Sampaolo, C. Yu, T. Wei, A. Zifarelli, M. Giglio, P. Patimisco, H. Zhu, H. Zhu, L. He, H. Wu, L. Dong, G. Xu, V. Spagnolo, H2S quartz-enhanced photoacoustic spectroscopy sensor employing a liquid-nitrogen-cooled THz quantum cascade laser operating in pulsed mode, Photoacoustics 21 (2021), 100219, https://doi.org/10.1016/J.PACS.2020.100219.
[29] M. Helman, H. Moser, A. Dudkowiak, B. Lendl, Off - beam quartz - enhanced photoacoustic spectroscopy - based sensor for hydrogen sulfide trace gas detection using a mode - hop - free external cavity quantum cascade laser, Appl. Phys. B 123 (2017) 1–8, https://doi.org/10.1007/s00340-017-6717-8.
[30] M.S. de Cumis, S. Viciani, S. Borri, P. Patimisco, A. Sampaolo, G. Scamarcio, P. De Natale, F. D'Amato, V. Spagnolo, Widely-tunable mid-infrared fiber-coupled quartz-enhanced photoacoustic sensor for environmental monitoring, Opt. Express 22 (2014) 28222–28231.
[31] A.A. Kosterev, L. Dong, D. Thomazy, F.K. Tittel, S. Overby, QEPAS for chemical analysis of multi-component gas mixtures, Appl. Phys. B 101 (2010) 649–659.
[32] H. Wu, A. Sampaolo, L. Dong, P. Patimisco, X. Liu, H. Zheng, X. Yin, L. Zhang, W. Yin, V. Spagnolo, S. Jia, F.K. Tittel, H. Wu, A. Sampaolo, L. Dong, P. Patimisco, X. Liu, A Custom Tuning Fork with Large Prong Spacing Quartz Enhanced Photoacoustic H 2 S Gas Sensor Based on a Fiber-amplifier Source and a Custom Tuning Fork with Large Prong Spacing, 111104 (2015) 2–6. doi: 10.1063/1.4930995.
[33] C. Feng, M. Giglio, L. Biao, A. Sampaolo, P. Patimisco, V. Spagnolo, D. Lei, H. Wu, Detection of hydrogen sulfide in sewer using an erbium-doped fiber amplified diode laser and a gold-plated photoacoustic cell, Molecules (2022).
[34] S. Viciani, M. de Cumis, S. Borri, P. Patimisco, A. Sampaolo, G. Scamarcio, P. De Natale, F. D'Amato, V. Spagnolo, A quartz-enhanced photoacoustic sensor for H2S trace-gas detection at 2.6 μm, Appl. Phys. B 119 (2015) 21–27.
[35] O.N. Ulenikov, E.S. Bekhtereva, S. Albert, S. Bauerecker, H.M. Niederer, M. Quack, Survey of the high resolution infrared spectrum of methane (12CH4 and 13CH4): partial vibrational assignment extended towards 12 000 cm-1, J. Chem. Phys. 141 (2014), https://doi.org/10.1063/1.4899263.
[36] S. Dello Russo, A. Sampaolo, P. Patimisco, G. Menduni, M. Giglio, C. Hoelzl, V.M. N. Passaro, H. Wu, L. Dong, V. Spagnolo, Quartz-enhanced photoacoustic spectroscopy exploiting low-frequency tuning forks as a tool to measure the vibrational relaxation rate in gas species, Photoacoustics 21 (2021), 100227, https://doi.org/10.1016/j.pacs.2020.100227.
[37] A.A. Kosterev, Y.A. Bakhirkin, F.K. Tittel, S. McWhorter, B. Ashcraft, QEPAS methane sensor performance for humidified gases, Appl. Phys. B Lasers Opt. 92 (2008) 103–109, https://doi.org/10.1007/s00340-008-3056-9.
[38] A. Elefante, G. Menduni, H. Rossmadl, V. Mackowiak, M. Giglio, A. Sampaolo, P. Patimisco, V.M.N. Passaro, V. Spagnolo, Environmental monitoring of methane with quartz-enhanced photoacoustic spectroscopy exploiting an electronic hygrometer to compensate the h2o influence on the sensor signal, Sensors 20 (2020), https://doi.org/10.3390/s20102935.
[39] H. Wu, L. Dong, X. Yin, A. Sampaolo, P. Patimisco, W. Ma, L. Zhang, W. Yin, L. Xiao, V. Spagnolo, S. Jia, Atmospheric CH4 measurement near a landfill using an ICL-based QEPAS sensor with V-T relaxation self-calibration, Sens. Actuators B Chem. 297 (2019), 126753, https://doi.org/10.1016/j.snb.2019.126753.
[40] N. Barreiro, A. Peuriot, G. Santiago, V. Slezak, Water-based enhancement of the resonant photoacoustic signal from methane–air samples excited at 3.3 μm, Appl. Phys. B. 108 (2012) 369–375, https://doi.org/10.1007/s00340-012-5018-5.
[41] J. Finzi, F.E. Hovis, V.N. Panfilov, P. Hess, C. Bradley Moore, Vibrational relaxation of water vapor, J. Chem. Phys. 67 (1977) 4053–4061, https://doi.org/10.1063/1.435379.
[42] S. Schilt, J.P. Besson, L. Thévenaz, Near-infrared laser photoacoustic detection of methane: the impact of molecular relaxation, Appl. Phys. B Lasers Opt. 82 (2006) 319–329, https://doi.org/10.1007/s00340-005-2076-y.
[43] N. Barreiro, A. Vallespi, G. Santiago, V. Slezak, A. Peuriot, Influence of oxygen on the resonant photoacoustic signal from methane excited at the ν 3 mode, Appl. Phys. B Lasers Opt. 104 (2011) 983–987, https://doi.org/10.1007/s00340-011-4546-8.
[44] H.C. Allen, E.K. Plyler, Infrared spectrum of hydrogen sulfide, J. Chem. Phys. 25 (1956) 1132–1136, https://doi.org/10.1063/1.1743164.
[45] L.R. Brown, J.A. Crisp, D. Crisp, O.V. Naumenko, M.A. Smirnov, L.N. Sinitsa, A. Perrin, The absorption spectrum of H2S between 2150 and 4260 cm- 1: analysis of the positions and intensities in the first (2ν2, ν1, and ν3) and second (3ν2, ν1+ ν2, and ν2+ ν3) triad regions, J. Mol. Spectrosc. 188 (1998) 148–174. ⟨https://www.sciencedirect.com/science/article/pii/S0022285297975019⟩. accessed May 20, 2022.
[46] H.-J. Bauer, A.C.C. Paphitis, R. Schotter, Vibrational and rotational relaxation in hydrogen sulfide, Physica 47 (1970) 109–112, https://doi.org/10.1016/0031-8914(70)90104-7.
[47] H. Bauer, A. Paphitis, R.S.- Physica, U. 1970, Vib-Vib transitions in mixtures of methane and hydrogen sulfide compared with those in the system methane-water vapour, Elsevier. 47 (1970) 58–63. ⟨https://www.sciencedirect.com/science/article/pii/0031891470900996⟩. (Accessed 20 May 2022).
[48] P. Patimisco, A. Sampaolo, M. Giglio, S. dello Russo, V. Mackowiak, H. Rossmadl, A. Cable, F.K. Tittel, V. Spagnolo, Tuning forks with optimized geometries for quartz-enhanced photoacoustic spectroscopy, Opt. Express 27 (2019) 1401–1415, https://doi.org/10.1364/OE.27.001401.
[49] Hitran Database, (n.d.). ⟨https://hitran.org/⟩.
[50] M. Giglio, P. Patimisco, A. Sampaolo, G. Scamarcio, F.K. Tittel, V. Spagnolo, Allan deviation plot as a tool for quartz-enhanced photoacoustic sensors noise analysis, IEEE Trans. Ultrason. Ferroelectr. Freq. Control. 63 (2016) 555–560, https://doi.org/10.1109/TUFFC.2015.2495013.
[51] A. Sampaolo, P. Patimisco, M. Giglio, A. Zifarelli, H. Wu, L. Dong, V. Spagnolo, Quartz-enhanced photoacoustic spectroscopy for multi-gas detection: a review, Anal. Chim. Acta (2021), 338894.
[52] H. Hosaka, K. Itao, S. Kuroda, Damping characteristics of beam-shaped micro-oscillators, Sens. Actuators A Phys. 49 (1995) 87–95, https://doi.org/10.1016/0924-4247(95)01003-J.
[53] P. Patimisco, A. Sampaolo, L. Dong, M. Giglio, G. Scamarcio, F.K. Tittel, V. Spagnolo, Analysis of the electro-elastic properties of custom quartz tuning forks for optoacoustic gas sensing, Sens. Actuators B Chem. 227 (2016) 539–546, https://doi.org/10.1016/j.snb.2015.12.096.
[54] P. Patimisco, A. Sampaolo, V. Mackowiak, H. Rossmadl, A. Cable, F.K. Tittel, V. Spagnolo, Loss mechanisms determining the quality factors in Quartz tuning forks vibrating at the fundamental and first overtone modes, IEEE Trans. Ultrason. Ferroelectr. Freq. Control. 65 (2018) 1951–1957, https://doi.org/10.1109/TUFFC.2018.2853404.
[55] M. Olivieri, A. Zifarelli, G. Menduni, M. Di Gioia, C. Marzocca, V.M.N. Passaro, A. Sampaolo, M. Giglio, V. Spagnolo, P. Patimisco, Influence of air pressure on the resonance properties of a t-shaped quartz tuning fork coupled with resonator tubes, Appl. Sci. 11 (2021), https://doi.org/10.3390/app11177974.
[56] S. Dello Russo, M. Giglio, A. Sampaolo, P. Patimisco, G. Menduni, H. Wu, L. Dong, V.M.N. Passaro, V. Spagnolo, Acoustic coupling between resonator tubes in Quartz-enhanced photoacoustic spectrophones employing a large prong spacing tuning fork, Sensors 19 (2019) 4109, https://doi.org/10.3390/S19194109.
[57] M. Müller, T. Rück, S. Jobst, J. Pangerl, S. Weigl, R. Bierl, F.M. Matysik, An algorithmic approach to compute the effect of non-radiative relaxation processes in photoacoustic spectroscopy, Photoacoustics 26 (2022), 100371, https://doi.org/10.1016/j.pacs.2022.100371.
[58] J. Pangerl, M. Müller, T. Rück, S. Weigl, R. Bierl, Characterizing a sensitive compact mid-infrared photoacoustic sensor for methane, ethane and acetylene detection considering changing ambient parameters and bulk composition (N2, O2 and H2O), Sens. Actuators B Chem. 352 (2022), 130962, https://doi.org/10.1016/j.snb.2021.130962.

Mariagrazia Olivieri obtained the M.S. degree (cum laude) in Physics in 2021 from the University of Bari. Since October 2021, she is a Ph.D. student at the Physics Department of the University of Bari carrying out her research work at PolySense Lab, joint-research laboratory between Technical University of Bari and THORLABS GmbH. Currently, her research activities are focused on the development of gas sensors based on Quartz Enhanced Photoacoustic spectroscopy for the analysis of complex gas mixtures.

Giansergio Menduni received the M.S. degree (cum laude) in Electronic Engineering in 2017 from the Technical University of Bari. Since 2018, he is a Ph.D. student at the Electric and Information Engineering Department of Polytechnic of Bari. Since 2022, he is an Assistant Professor in Applied Physics at the Physics Department of Polytechnic of Bari. His research activity is focused on the development of gas sensors based on Quartz Enhanced Photoacoustic Spectroscopy.

Marilena Giglio received the M.S. degree (cum laude) in Applied Physics in 2014, and the Ph.D. Degree in Physics in 2018 from the University of Bari. Since 2021, she is a Assistant Professor at the Physics Department of the Technical University of Bari. Her research activity is focused on the development of gas sensors based on Quartz-Enhanced Photoacoustic Spectroscopy and on the optical coupling of hollow-core waveguides with interband- and quantum-cascade lasers.

Angelo Sampaolo obtained his Master degree in Physics in 2013 and the Ph.D. Degree in Physics in 2017 from University of Bari. He was an associate researcher in the Laser Science Group at Rice University from 2014 to 2016 and associate researcher at Shanxi University since 2018. Since 2019, he is Assistant Professor at Polytechnic of Bari. His research activity has focused on the development of innovative techniques in trace gas sensing, based on Quartz-Enhanced Photoacoustic Spectroscopy and covering the full spectral range from near-IR to THz.

Pietro Patimisco obtained the Master degree in Physics (cum laude) in 2009 and the Ph.D. Degree in Physics in 2013 from the University of Bari. Since 2018, he is Assistant professor at the Technical University of Bari. Dr. Patimisco's scientific activity addressed the study and applications of trace-gas sensors, such as quartz-enhanced photoacoustic spectroscopy and cavity enhanced absorption spectroscopy in the mid infrared and terahertz spectral region, leading to several publications.

Hongpeng Wu received his Ph.D. degree in atomic and molecular physics from Shanxi University, China, in 2017. From September, 2015 to October, 2016, he studied as a joint Ph.D. student in the Electrical and Computer Engineering Department and Rice Quantum Institute, Rice University, Houston, USA. Currently he is a professor in the Institute of Laser Spectroscopy of Shanxi University. His research interests include gas sensors, photoacoustic spectroscopy, photothermal spectroscope and laser spectroscopy techniques.

Lei Dong received his Ph.D. degree in optics from Shanxi University, China, in 2007. From June, 2008 to December, 2011, he worked as a post-doctoral fellow in the Electrical and Computer Engineering Department and Rice Quantum Institute, Rice University, Houston, USA. Currently he is a professor in the Institute of Laser Spectroscopy of Shanxi University. His research interests include optical sensors, trace gas detection, photoacoustic spectroscopy and laser spectroscopy.

Vincenzo Spagnolo received the degree (summa cum laude) and the Ph.D., both in physics, from University of Bari. He works as Full Professor of Applied Physics at the Technical University of Bari. In 2019, he become Vice-Rector of the Technical University of Bari, deputy to Technology Transfer. Since 2017, he is the director of the joint-research lab PolySense, created by THORLABS GmbH and Technical University of Bari, devoted to the development and implementation of novel gas sensing techniques and the realization of highly sensitive QEPAS trace-gas sensors.